Supplementary Information for

Tuning the Co pre-oxidation process of Co_3O_4 via geometrically reconstructed F−Co−O active sites for boosting acidic water oxidation

Yi Wang,[‡, a, b, g] Pu Guo,[‡, a, g] Jing Zhou,[c] Bing Bai,[a, b, g] Yifan Li,[d, e] Mingrun Li,[a, g] Pratteek Das,[a, g] Xianhong Wu,[a, g] Linjuan Zhang,[c, f] Yi Cui,[d, e] Jianping Xiao,* [a, b, g] and Zhong-Shuai Wu* [a, b, g]

[a] *State Key Laboratory of Catalysis, Dalian Institute of Chemical Physics, Chinese Academy of Sciences, 457 Zhongshan Road, Dalian 116023, China*

[b] *University of Chinese Academy of Sciences, 19 A Yuquan Road, Shijingshan District, Beijing 100049, China*

[c] *Key Laboratory of Interfacial Physics and Technology, Shanghai Institute of Applied Physics, Chinese Academy of Sciences, Shanghai 201800, China*

[d] *Vacuum Interconnected Nanotech Workstation, Suzhou Institute of Nano-Tech and Nano-Bionics, Chinese Academy of Sciences, Suzhou, 215123, China*

[e] *School of Nano Technology and Nano Bionics University of Science and Technology of China, Hefei 230026, China*

[f] *Institute of Chemical and Engineering Sciences, A*STAR, Singapore 627833, Singapore*

[g] *Dalian National Laboratory for Clean Energy, Chinese Academy of Sciences, 457 Zhongshan Road, Dalian 116023, China*

† *Electronic Supplementary Information (ESI) available: See DOI: 10.1039/*x0xx00000x

‡ These authors contributed equally to this work.

*Corresponding author(s): xiao@dicp.ac.cn (J. P. Xiao); wuzs@dicp.ac.cn (Z.-S. Wu)

Materials and Methods

Synthesis of $Co_3O_{4-x}F_x$

First, 45 mg $Co(NO_3)_3 \cdot 6H_2O$ and 2.25 mg NH_4F were added in 100 μL H_2O and C_2H_5OH mixed solution, and then treated with sonication. Then, a 1 × 2 cm^2 hydrophilic carbon paper was placed on a hotplate under 90 °C. Next, the above mixture was sprayed on it, followed by calcination on a hotplate at 90 °C in the air for 2 h. Finally, the electrode precursor material was annealed in air at 400 °C for 2 h to obtain the $Co_3O_{4-x}F_x$ catalyst, with the doping content of ~7 wt%.

The Co_3O_4 catalyst was synthesized following a similar protocol without adding NH_4F.

Materials characterization

The SEM images and EDS were obtained on a JSM-7800F microscope. TEM, HRTEM, HAADF-STEM images, and elemental mapping images were taken with ARM300 microscope with a spherical aberration corrector. XRD data were collected on a SmartLab using Cu *K*α radiation. XPS spectra were conducted on the Hermo Scientific *K*-Alpha instrument. *Quasi in-situ* XPS spectra were collected at the SPECS NAP-XPS instrument attached to the glove box through a vacuum channel. Raman spectroscopy was recorded by Renishaw inVia confocal Raman microscope with excitation laser wavelength of 532 nm. TOF-SIMS measurements were performed using ABI MALDI TOF/TOF 5800 instrument. Elemental-specific XAS data were collected in the BL12B and BL14W1 beamlines of the Hefei National Synchrotron Radiation Laboratory (NSRL) and Shanghai Synchrotron Radiation Facility (SSRF) in China, respectively.

Electrochemical measurements

The electrochemical performance was tested on a CHI 760E workstation at ambient temperature and pressure. In a typical three-electrode system, a carbon paper (1 cm^2), the Hg/Hg_2SO_4 electrode and graphite rod were employed as the working, reference and counter electrodes, respectively. LSV curves were performed in an O_2-saturated 0.5 M H_2SO_4 solution at a scan rate of 10 mV s^{-1}, without *IR* drop compensation. The potentials measured were converted to reversible hydrogen electrode (RHE) according

to the following equation: $E_{RHE} = E_{Hg/Hg2SO4} + 0.059\ pH + 0.656$, where the pH value is 0.3 for the 0.5 M H_2SO_4 solution.

The measurement of PEM water electrolysis was performed on the self-made cell with membrane electrode assemblies (MEAs) at 50 °C, which mainly contains bipolar plate, gas diffusion layer (GDL), Nafion®117 polymer membrane (DuPont), commercial Pt/C (20 wt%) cathode catalyst and $Co_3O_{4-x}F_x$ catalyst. Specifically, around 1 mg cm^{-2} of Pt/C (20 wt%) catalyst was uniformly sprayed onto the polymer membrane as the cathode. For the anode, the OER catalyst of $Co_3O_{4-x}F_x$ was directly synthesized on carbon paper (TGP-H-060) with a loading of ~ 3 mg cm^{-2}. Carbon paper (AvCarb) and titanium felt are used as the GDL for the cathode and anode, respectively. And the chronopotentometric curve was not IR corrected.

Theoretical analysis.

All the DFT calculations were performed with the Vienna *ab* initio simulation package.[1] The optimized geometries of the computational models are shown in Table S4. The projector-augmented wave method was performed as the basis set with the cut-off energy of 400 eV and Perdew–Burke–Ernzerhof (PBE) exchange-correlation functional[2] was applied to the optimization of all structures. The effects of the Hubbard *U* corrections were considered, where *U* values (employed as $U - J$) of 3.0 were applied for Co.[3] The smearing (0.2 eV) based on the method of Methfessel–Paxton[4] was applied to the total energy calculations. The optimized lattice parameter a = b = c = 8.106 Å was used for Co_3O_4, which is consistent with the experimental measurements. The Monkhorst–Pack *k* points of 4 × 4 × 4 were applied for the bulk optimization of Co_3O_4 (24 Co atoms and 32 O atoms). The Co_3O_4 (311) surface was modeled by a slab of 4 layers with a (1 × 1) unit. The Co_3O_4(110) surface was modeled by a slab of 4 bi-layers with a (1 × 1) unit. The (311) and (110) surfaces were studied with Monkhorst–Pack *k* points of (1 × 2 × 1) and (3 × 2 × 1), respectively. We calculated the different F-doping sites and chose the most stable one (Table S4). The force convergence was set to 0.05 eV $Å^{-1}$. In addition, the computational hydrogen electrode approximation was used to describe the chemical potential of OH^- (Table S5) and free energies were corrected to the temperature of 298 K (Table S6). The implicit solvent effect was

considered.[5, 6]

We calculated the adsorption free energies of O*, OH* and OOH* on the eight active sites (Figure S22 and Table S5) of Co_3O_4 and $Co_3O_{4-x}F_x$. The adsorption free energies of O* (G_{ad} O*) and OOH* (G_{ad} OOH*) were chosen as descriptors to establish the two-dimensional maps (Figure S23).

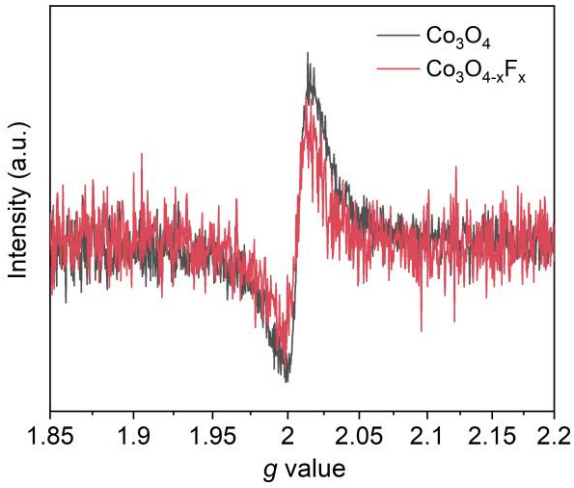

Fig. S1 EPR spectra of Co_3O_4 and $Co_3O_{4-x}F_x$.

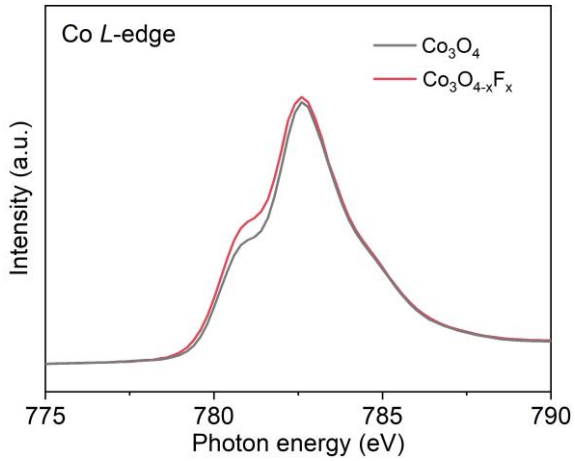

Fig. S2 Co *L*-edge XAS spectra of Co_3O_4 and $Co_3O_{4-x}F_x$.

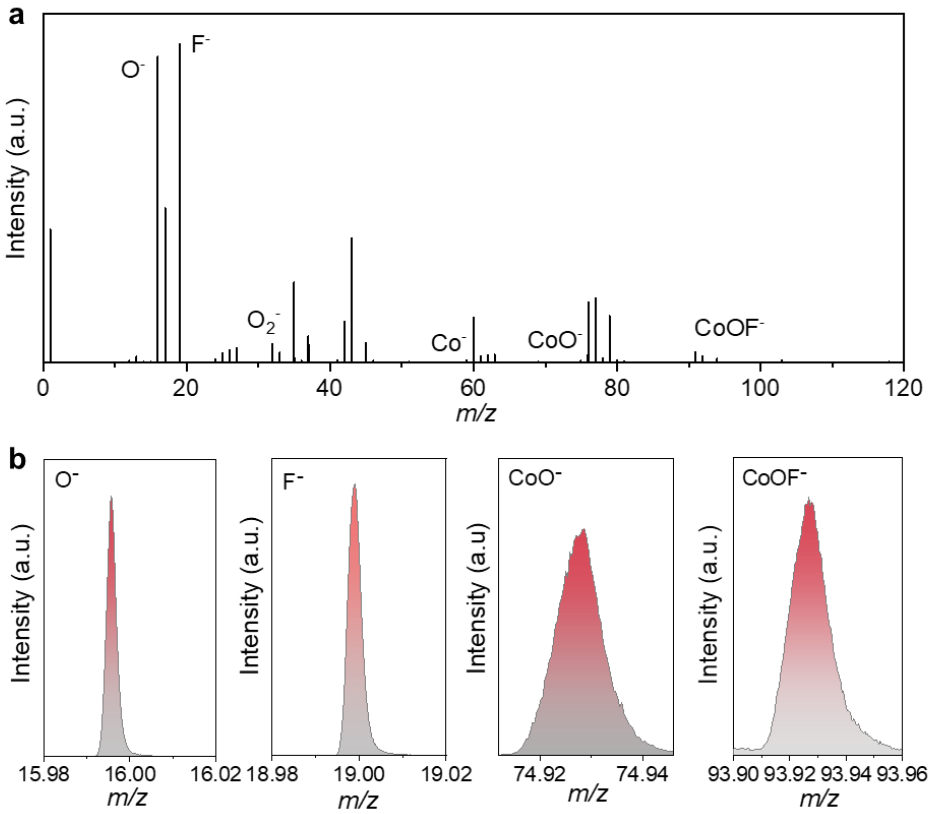

Fig. S3 TOF-SIMS spectra of $Co_3O_{4-x}F_x$.

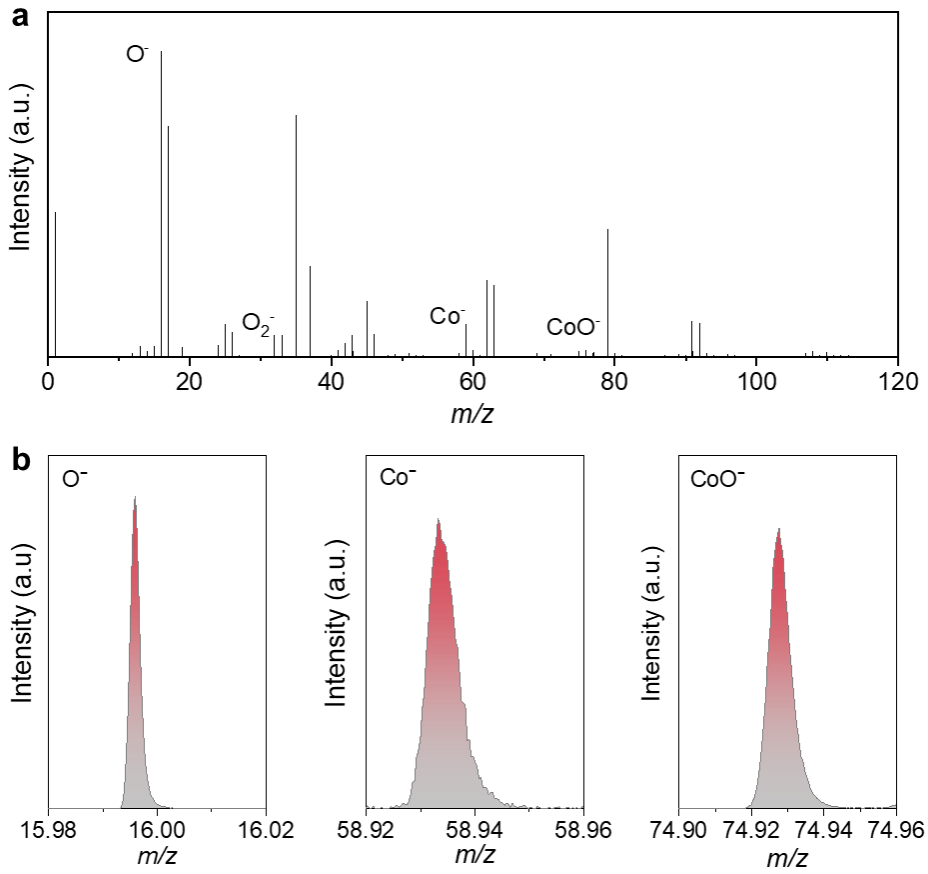

Fig. S4 TOF-SIMS spectra of Co_3O_4.

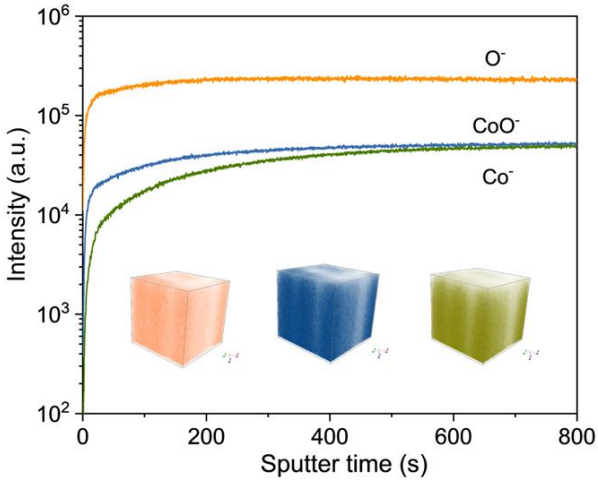

Fig. S5 Unnormalized TOF-SIMS depth profiles of O^-, Co^-, and CoO^- for Co_3O_4.

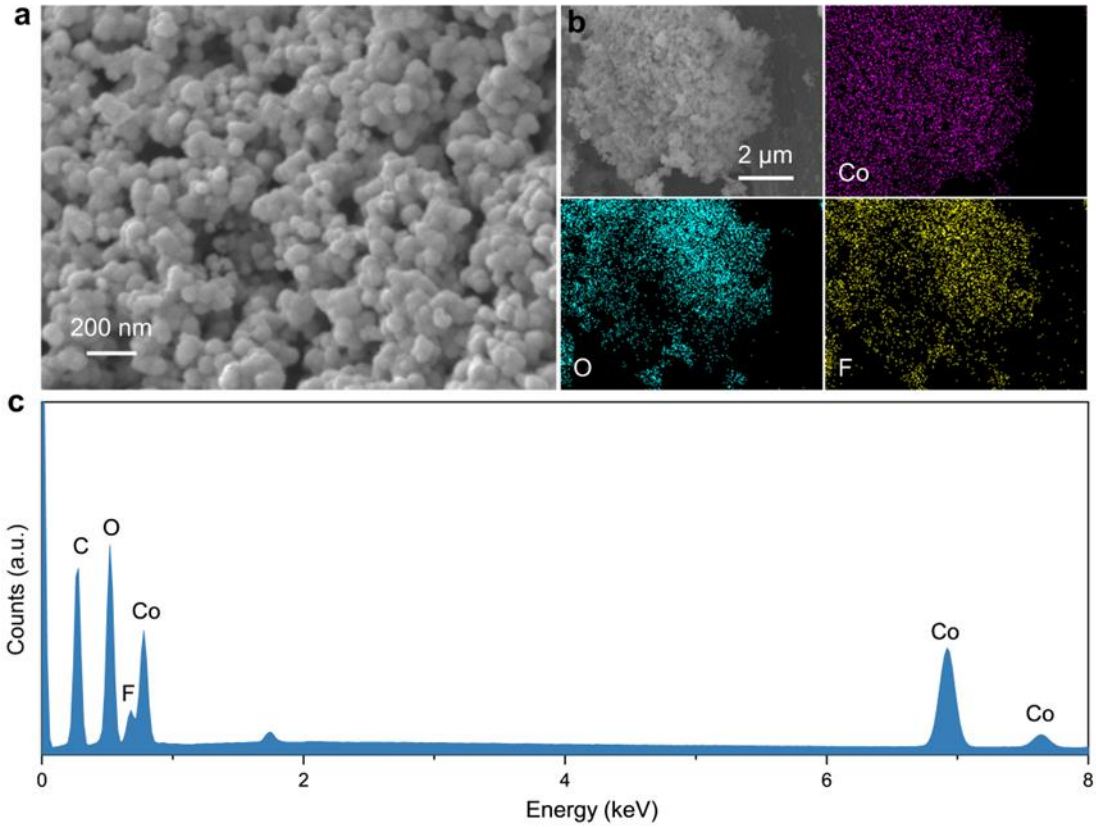

Fig. S6 (a-c) SEM image (a), elemental mapping images (b), and EDX spectrum (c) of $Co_3O_{4-x}F_x$.

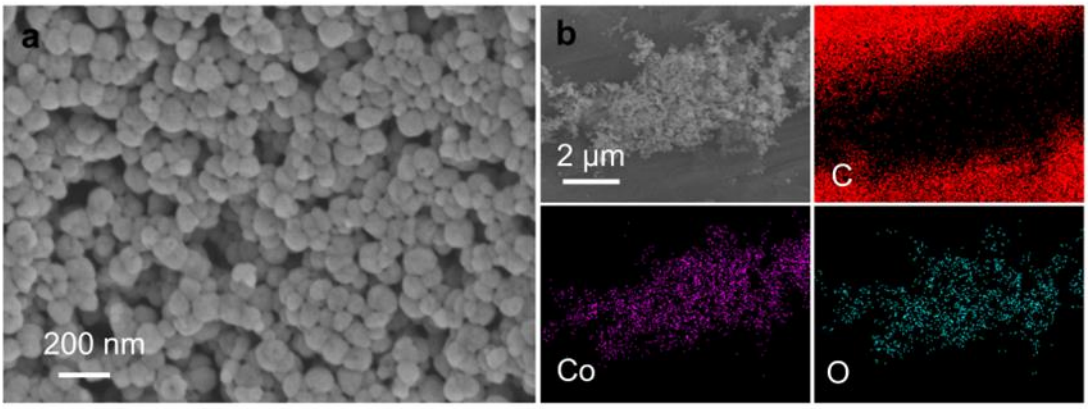

Fig. S7 (a, b) SEM image (a) and elemental mapping images (b) of the Co_3O_4.

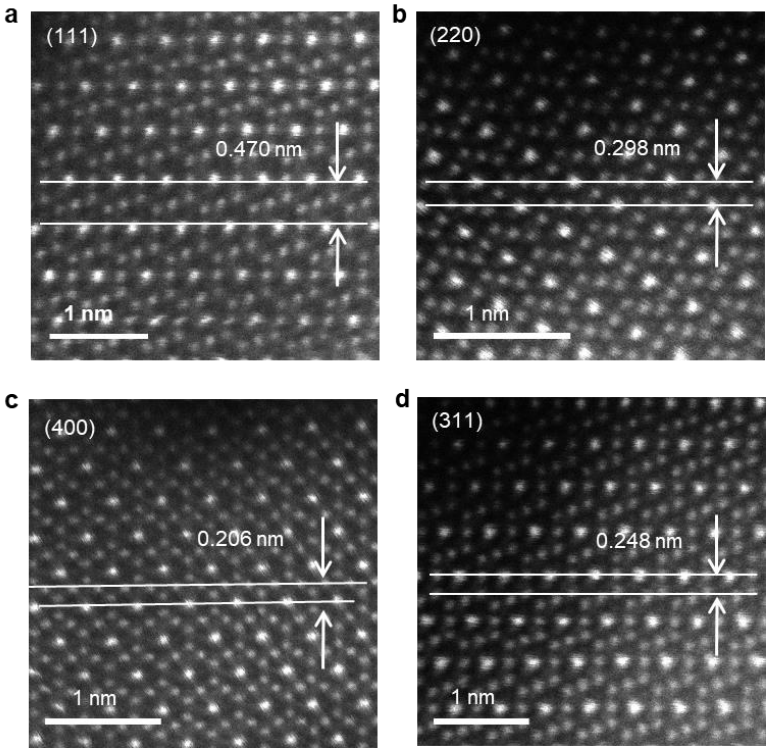

Fig. S8 HAADF-STEM image of (111, a), (220, b), (400, c) and (311, d) crystal planes for $Co_3O_{4-x}F_x$.

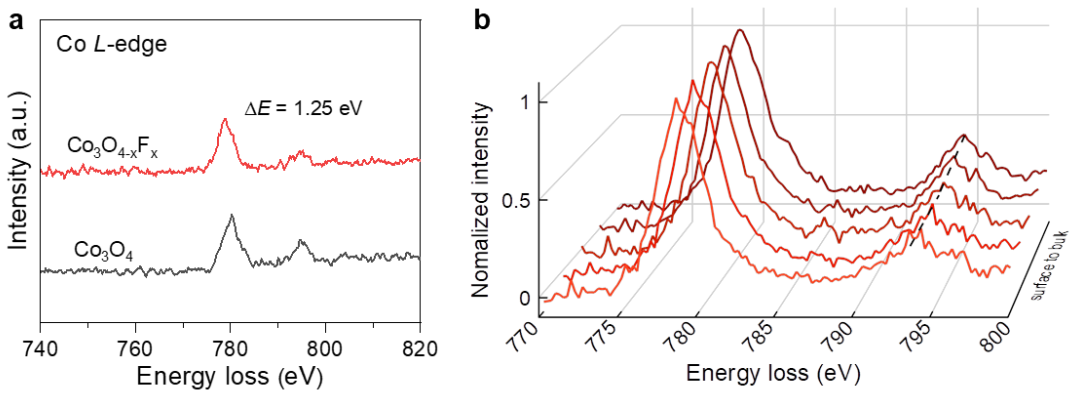

Fig. S9 (a) EELS spectra of Co *L*-edges of Co_3O_4 and $Co_3O_{4-x}F_x$. (b) The EELS spectra of Co *L*-edges from surface to bulk for $Co_3O_{4-x}F_x$.

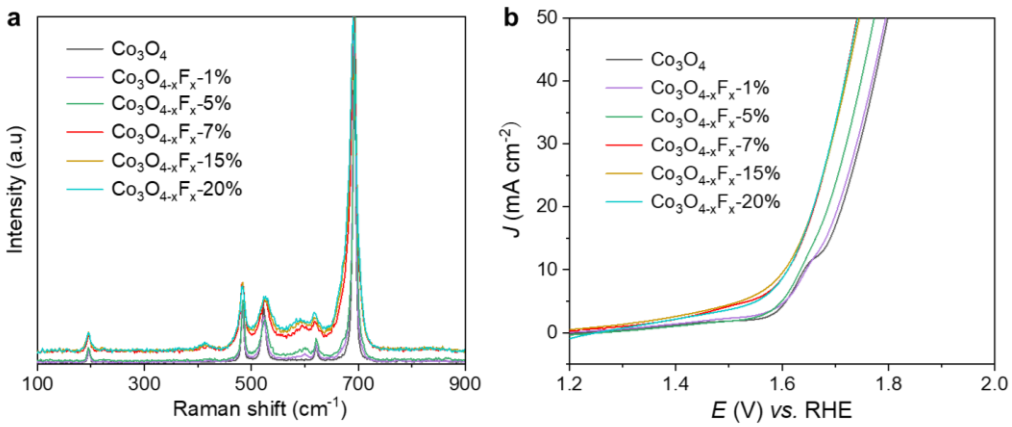

Fig. S10 (a, b) The Raman spectra (a) and LSV curves without *IR* correction (b) of Co_3O_4 and $Co_3O_{4-x}F_x$ with different F content.

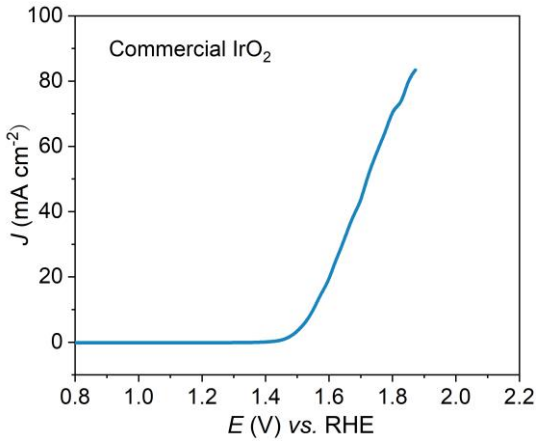

Fig. S11 LSV polarization curve of commercial IrO_2 without *IR* correction.

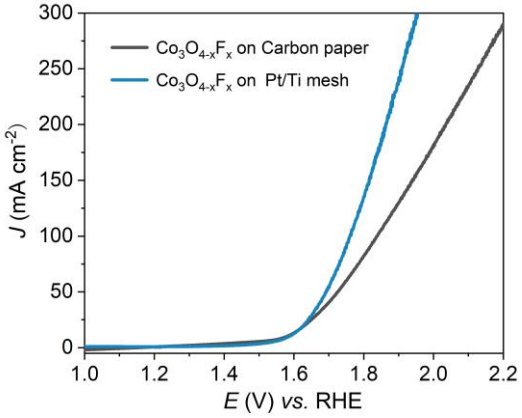

Fig. S12 LSV polarization curves of $Co_3O_{4-x}F_x$ on carbon paper or Pt/Ti mesh support without *IR* correction.

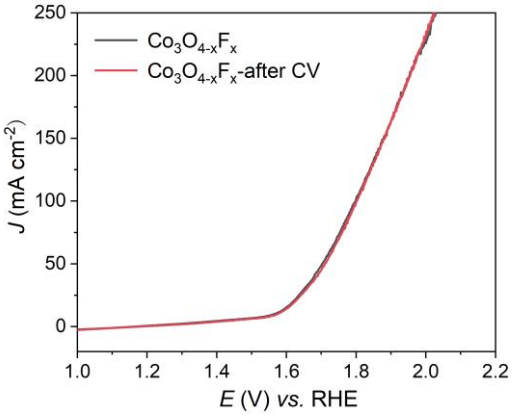

Fig. S13 LSV polarization curves of $Co_3O_{4-x}F_x$ before and after 2000 cycles potential cycling during OER without *IR* correction.

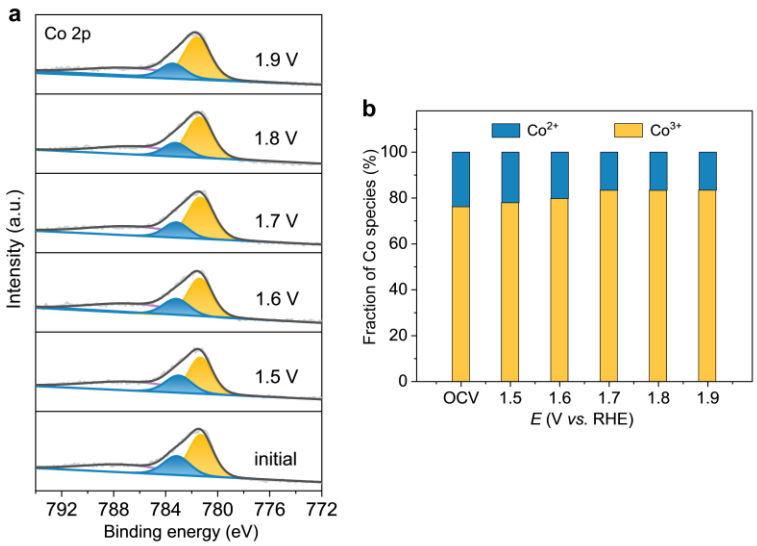

Fig. S14 (a) The *quasi in-situ Co 2p* XPS spectra recorded of the resultant Co_3O_4 during the multi-potential steps. (b) Fraction of Co species recorded of the resultant Co_3O_4 from *quasi in-situ Co 2p* XPS spectra (a).

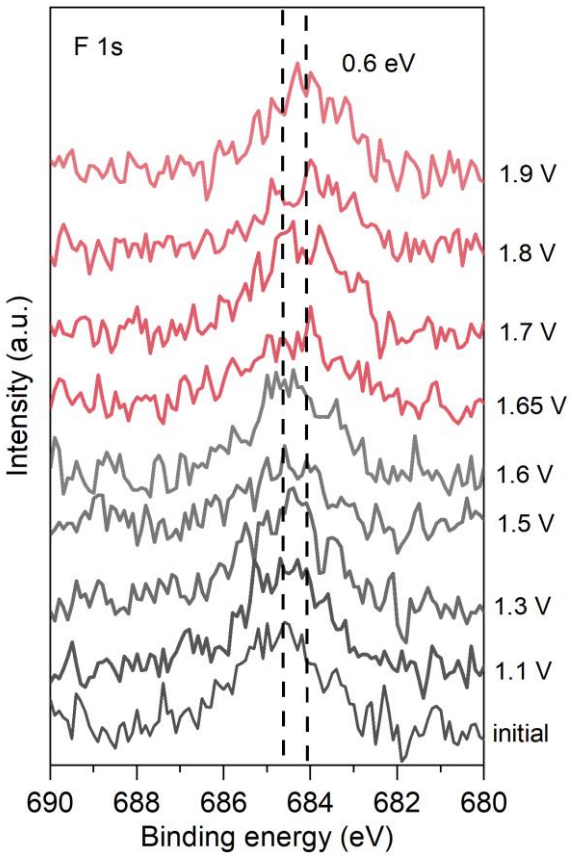

Fig. S15 The *quasi in-situ F 1s* XPS spectra recorded of the resultant $Co_3O_{4-x}F_x$ during the multi-potential steps.

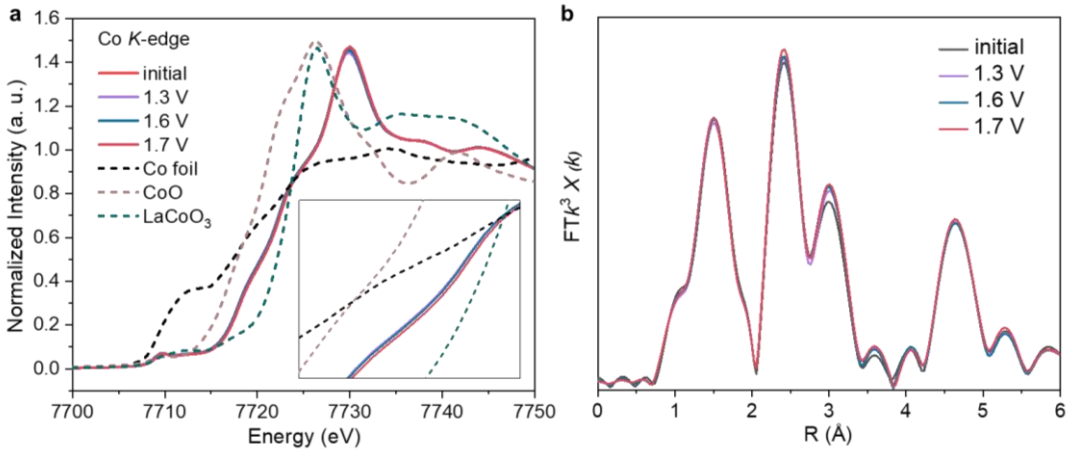

Fig. S16 (a, b) *Ex-situ* XAS (a) and FT-EXAFS (b) spectra of change of the Co *K*-edge for Co_3O_4 recorded during the multi-potential steps.

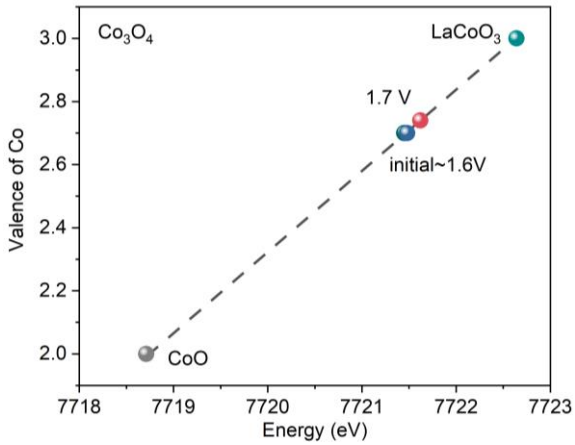

Fig. S17 Co oxidation state as a function of absorption edge energy for Co_3O_4 during the multi-potential steps.

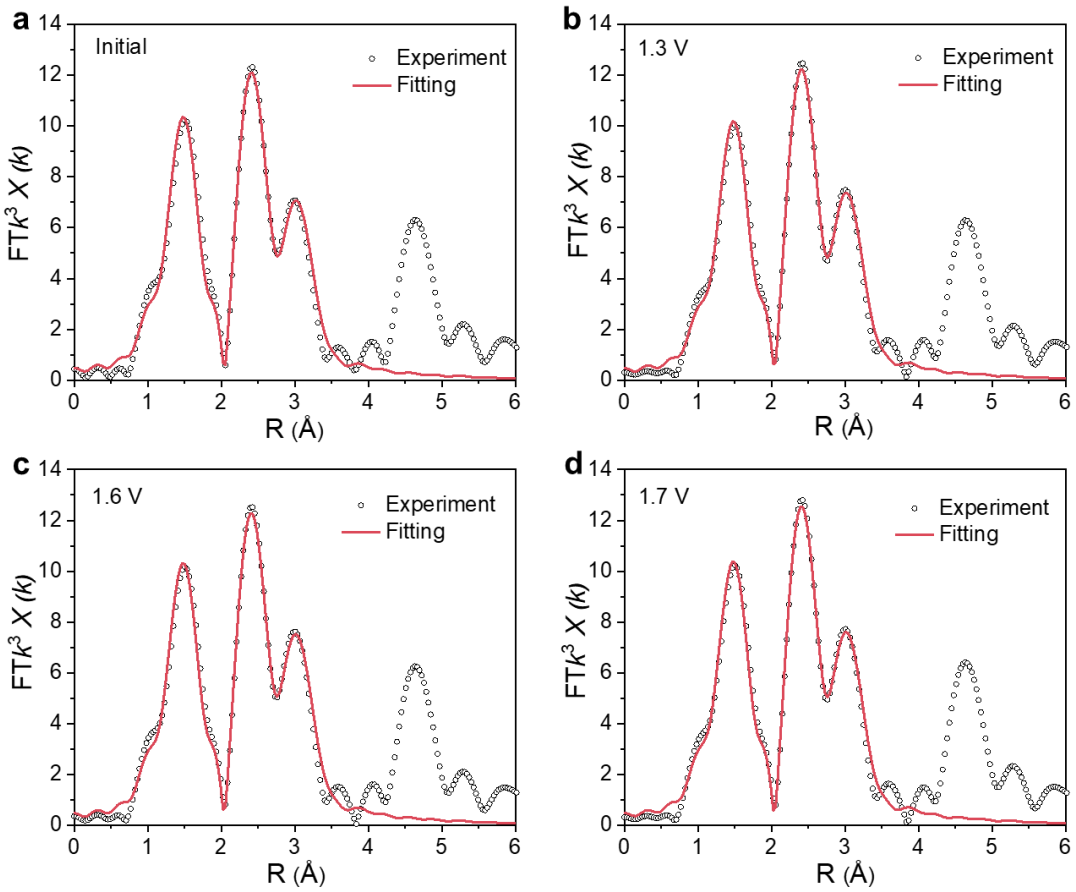

Fig. S18 k^3-weighted R-space Co *K*-edge experimental and fitting spectra of Co_3O_4 during the multi-potential steps.

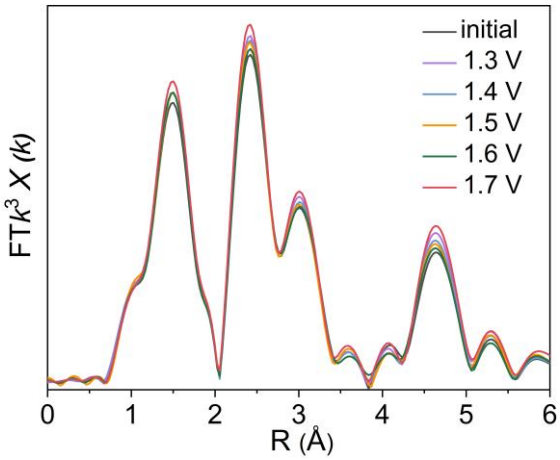

Fig. S19 *Ex-situ* FT-EXAFS spectra of the Co *K*-edge for $Co_3O_{4-x}F_x$ recorded during the multi-potential steps.

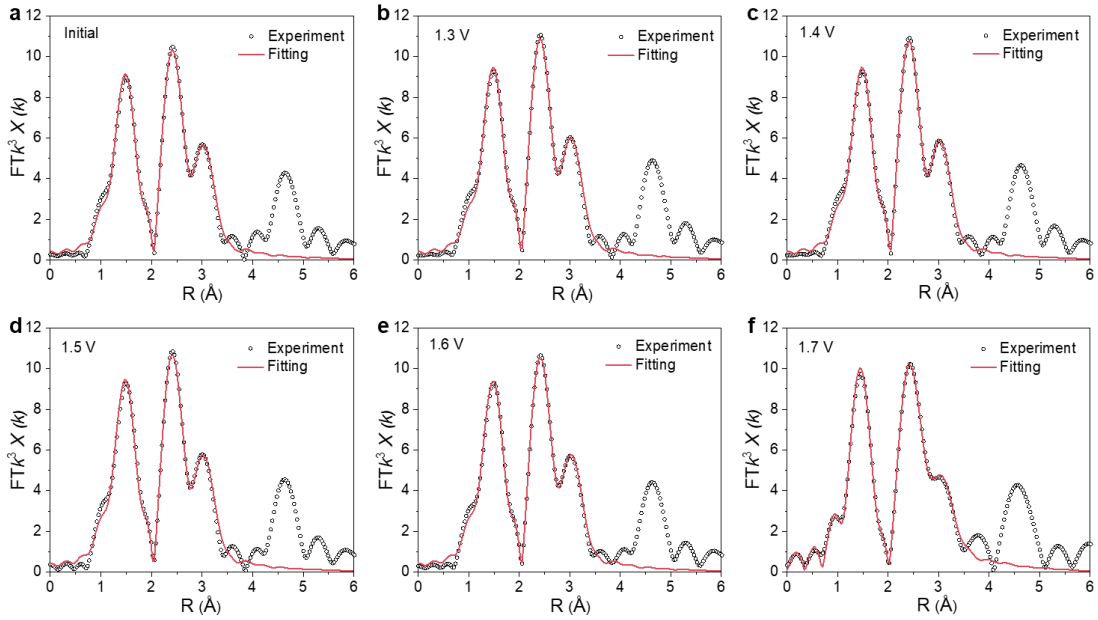

Fig. S20 k^3-weighted R-space Co *K*-edge experimental and fitting spectra of $Co_3O_{4-x}F_x$ during the multi-potential steps.

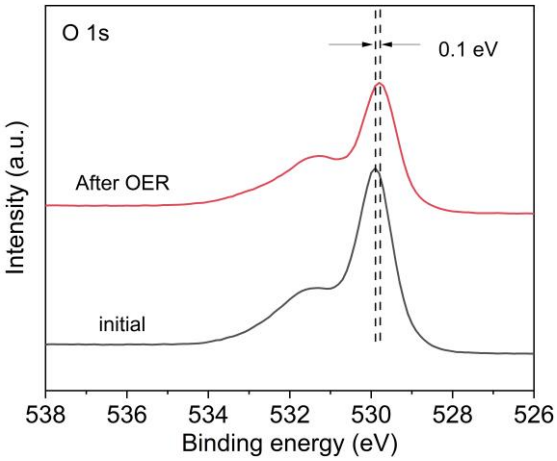

Fig. S21 *Ex-situ O 1s* XPS spectra of $Co_3O_{4-x}F_x$.

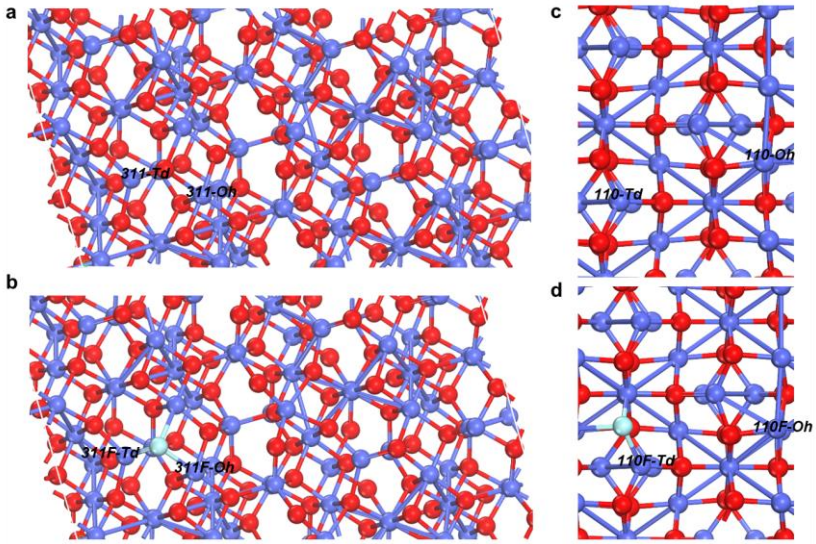

Fig. S22 The considered active sites for OER on pristine Co_3O_4 and $Co_3O_{4-x}F_x$. (a) 311-Oh and 311-Td denote the octahedral and tetrahedral Co sites on pristine Co_3O_4 (311) surface, respectively. (b) 311F-Oh and 311F-Td denote the octahedral and tetrahedral Co sites on $Co_3O_{4-x}F_x$ (311) surface, respectively. (c) 110-Oh and 110-Td denote the octahedral and tetrahedral Co sites on pristine Co_3O_4 (110) surface, respectively. (d) 110F-Oh and 110F-Td denote the octahedral and tetrahedral Co sites on $Co_3O_{4-x}F_x$ (110) surface, respectively. Blue, red and cyan balls represent the Co, O and F atoms, respectively.

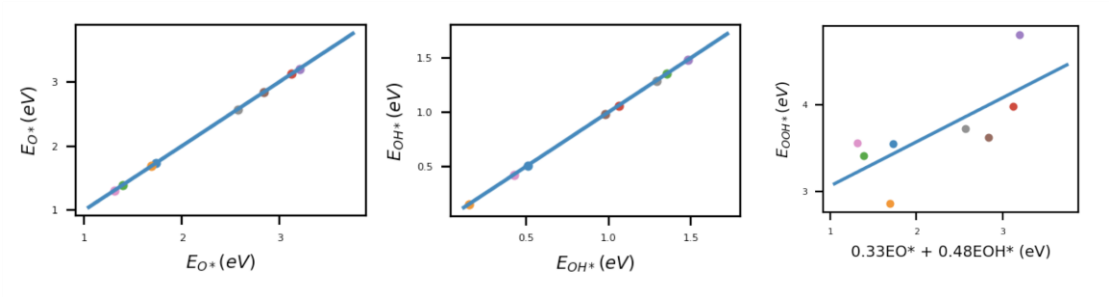

Fig. S23 The scaling relationship between the adsorption energies of O*, OH* and OOH* on diverse active sites of pristine Co_3O_4 and $Co_3O_{4-x}F_x$.

Table S1. EXAFS fitting parameters of $Co_3O_{4-x}F_x$ during the multi-potential steps

Sample	bond type	CN*	*R* (Å)	σ^2 (10^{-3}Å^2)**	R factor
Co-foil	Co-Co	12	2.49±0.01	6.2±0.7	0.007
	Co-O	4.7±0.4	1.92±0.01	3.2±0.7	
initial	Co-Co	4.8±0.3	2.87±0.01	5.6±1.5	0.003
	Co-Co	6.2±0.6	3.37±0.01	6.4±2.0	
	Co-O	4.8±0.4	1.92±0.01	3.1±0.6	
1.3 V	Co-Co	5.1±0.4	2.87±0.01	5.5±1.5	0.003
	Co-Co	6.5±0.7	3.38±0.01	6.4±1.3	
	Co-O	4.9±0.4	1.92±0.01	3.1±0.4	
1.4 V	Co-Co	5.1±0.2	2.87±0.01	5.6±1.5	0.002
	Co-Co	6.5±0.3	3.38±0.01	6.6±1.0	
	Co-O	4.8±0.2	1.92±0.01	3.1±0.3	
1.5 V	Co-Co	5.0±0.2	2.87±0.01	5.6±1.7	0.004
	Co-Co	6.2±0.3	3.37±0.01	6.4±0.8	
	Co-O	4.8±0.2	1.92±0.01	3.1±0.3	
1.6 V	Co-Co	5.0±0.2	2.87±0.01	5.6±1.5	0.003
	Co-Co	6.4±0.3	3.38±0.01	6.5±1.6	
	Co-O	5.0±0.2	1.92±0.01	3.1±0.3	
1.7 V	Co-Co	6.3±0.2	2.86±0.01	5.7±1.7	0.003
	Co-Co	6.5±0.3	3.38±0.01	6.5±2.2	

* CN: coordination number; S_0^2 was fixed to be 0.76 from Co-foil.

** σ^2: Debye−Waller factors

Table S2. EXAFS fitting parameters of Co_3O_4 during the multi-potential steps

Sample	bond type	CN*	*R* (Å)	σ^2 (10^{-3}Å^2)**	R factor
Co-foil	Co-Co	12	2.49±0.01	6.2±0.7	0.007
	Co-O	5.2±0.3	1.92±0.01	3.0±0.4	
initial	Co-Co	5.5±0.3	2.87±0.01	5.4±0.3	0.006
	Co-Co	7.7±0.5	3.37±0.01	6.6±0.4	
	Co-O	5.1±0.2	1.92±0.01	2.9±0.3	
1.3 V	Co-Co	5.4±0.2	2.87±0.01	5.3±0.3	0.004
	Co-Co	7.9±0.4	3.37±0.01	6.5±0.4	
	Co-O	5.2±0.2	1.92±0.01	2.9±0.3	
1.6 V	Co-Co	5.5±0.2	2.87±0.01	5.4±0.3	0.005
	Co-Co	8.1±0.4	3.38±0.01	6.5±0.4	
	Co-O	5.3±0.2	1.92±0.01	2.9±0.3	
1.7 V	Co-Co	5.7±0.2	2.86±0.01	5.3±0.3	0.004
	Co-Co	8.3±0.4	3.37±0.01	6.5±0.3	

* CN: coordination number; S_0^2 was fixed to be 0.76 from Co-foil.

** σ^2: Debye−Waller factors

Table S3. Performance comparison of $Co_3O_{4-x}F_x$ with the reported non-noble metal based OER catalysts

Catalyst	η_{10} (mV)	Stability performance	Electrolyte	Refs.
$Co_3O_{4-x}F_x$	349	120 h @100 mA cm^{-2}	0.5 M H_2SO_4	This work
$Co_{3-x}Ba_xO_4$	278	100 h @10 mA cm^{-2}	0.5 M H_2SO_4	7
Co_3O_4@C/GPO	398	40 h @10 mA cm^{-2}	1 M H_2SO_4	8
Ba[Co-POM]/CP	361	24 h @1 mA cm^{-2}	1 M H_2SO_4	9
Co_2TiO_4	513	10 h @1.79 V vs. RHE	0.5 M H_2SO_4	10
Co_3O_4-CeO_2	423	100 h @10 mA cm^{-2}	0.5 M H_2SO_4	11
$CoFePbO_x$	700	12 h @12 mA cm^{-2}	0.1 M H_2SO_4	12
LMCF	353	360 h @10 mA cm^{-2}	0.1 M $HClO_4$	13
Co_2MnO_4 on FTO	395	320 h @100 mA cm^{-2}	0.0 M H_2SO_4	14
Co_2MnO_4 on Pt/Ti mesh	298	1500 h @200 mA cm^{-2}	0.5 M H_2SO_4	14
γ-MnO_2	~440	1000 h @200 mA cm^{-2}	1 M H_2SO_4	15
$Mn_{7.5}O_{10}Br_3$	295±5	500 h @10 mA cm^{-2}	0.5 M H_2SO_4	16
$Ni_{0.5}Mn_{0.5}Sb_{1.7}O_y$	672±9	168 h @10 mA cm^{-2}	1 M H_2SO_4	17
$Mn_{0.8}Nb_{0.2}O_2$:10F	680	25 h @1.9 V vs. RHE	0.5 M H_2SO_4	18
NiFeP	540	30 h @10 mA cm^{-2}	0.05 M H_2SO_4	19
F-doped $Cu_{1.5}Mn_{1.5}O_4$	320	24 h @16 mA cm^{-2}	pH 0.3 H_2SO_4	20
1T-MoS_2	420	2 h @10 mA cm^{-2}	pH 0.3 H_2SO_4	21
NiFe@MoS_2	201	100 h @150 mA cm^{-2}	0.5 M H_2SO_4	22

Table S4. Total energies for F doping at different site on Co_3O_4 (311) surface. O_{2c}, O_{3c} and O_{4c} denote the 2-fold, 3-fold and 4-fold coordinated oxygen atom. Blue, red, cyan and white balls denote the Co, O, F and H atoms, respectively.

Geometry	O_{2c}	O_{3c}	O_{4c}
	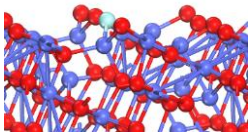	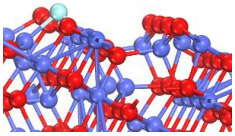	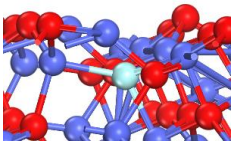
Total Energy	-1065.107331	-1065.190176	-1063.808170

Table S5. Reaction free energy calculations

Elementary steps	Free energy (ΔG)
(R0) $H_2O(l) + * \rightarrow OH^* + (H^+ + e^-)$	G_{OH*}
(R1) $OH^* \rightarrow O^* + (H^+ + e^-)$	$G_{O*} - G_{OH*}$
(R2) $O^* + H_2O(l) \rightarrow OOH^* + (H^+ + e^-)$	$G_{OOH*} - G_{O*}$
(R3) $OOH^* \rightarrow O_2(g) + (H^+ + e^-)$	$4.92 - G_{OOH*}$
(R4) $2O^* \rightarrow O_2(g) + 2^*$	$4.92 - 2G_{O*}$

The adsorption free energies of the three adsorbates (O*, OH* and OOH*) were calculated with reference to the gas-phase energies of H_2O and H_2. The reaction free energy at 0 V versus RHE can be calculated according to the Table S5.

What's more, elementary steps (R0-R3) are electrochemical steps and thus the reaction free energy of these steps is highly influenced by the electrode potential. The free energy of the potential-dependent reaction can be calculated by the computational hydrogen electrode approximation:

$$\Delta G_U = G_{U_0} + e(U - U_0)$$

Table S6. The corrections of zero-point energy and entropy of adsorbed species. All energies are in eV. (T = 298.15 K)

Species / Active sites	O*	OH*	OOH*
110-Oh	0.07	0.40	0.40
110-Td	0.02	0.26	0.4
110F-Oh	0.07	0.40	0.40
110F-Td	0.02	0.26	0.4
311-Oh	0.05	0.32	0.40
311-Td	0.03	0.28	0.36
311F-Oh	0.04	0.32	0.40
311F-Td	0.03	0.28	0.36

Table S7. The optimized geometries of O*, OH* and OOH* on diverse active sites.

Blue, red, green and pink balls denote the Co, O, F and H atoms.

	O*	OH*	OOH*
311-Oh	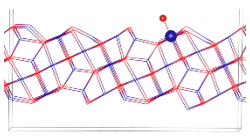	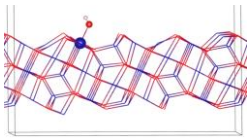	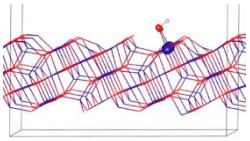
311-Td	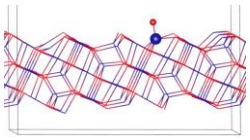	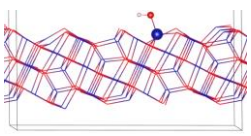	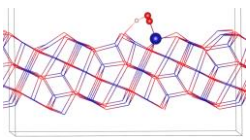
311F-Oh	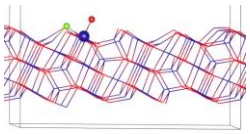	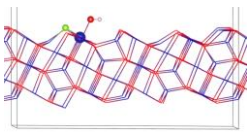	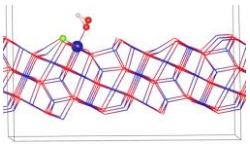
311F-Td	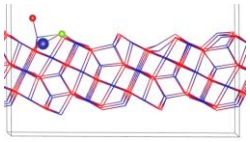	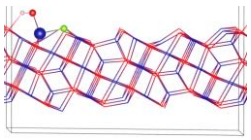	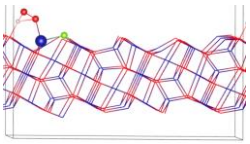
110-Oh	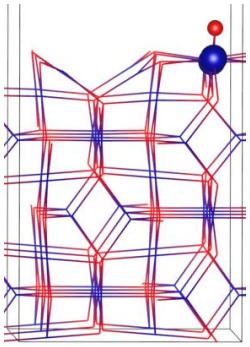	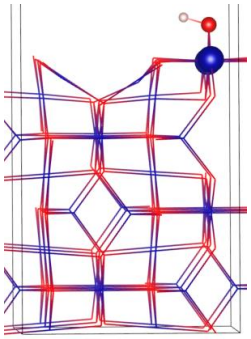	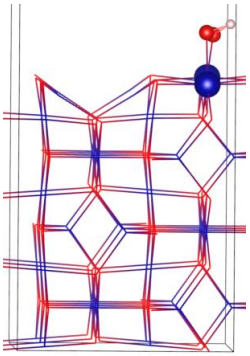
110-Td	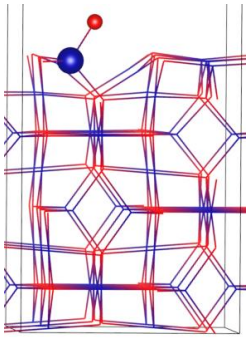	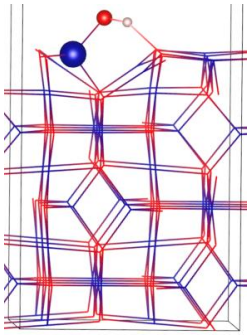	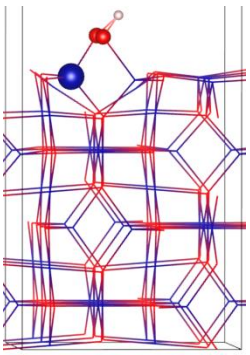

110F-Oh

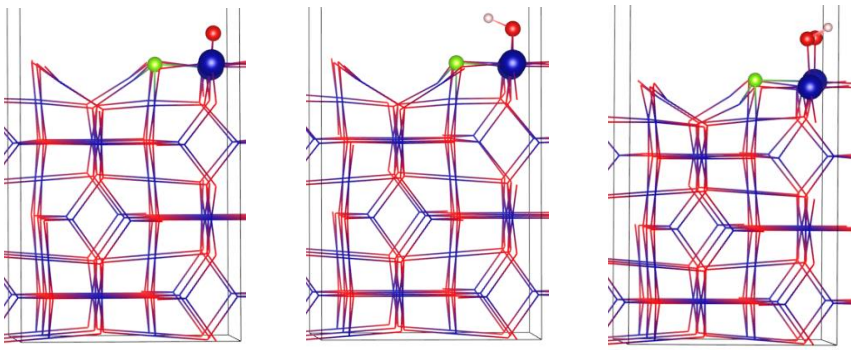

110F-Td

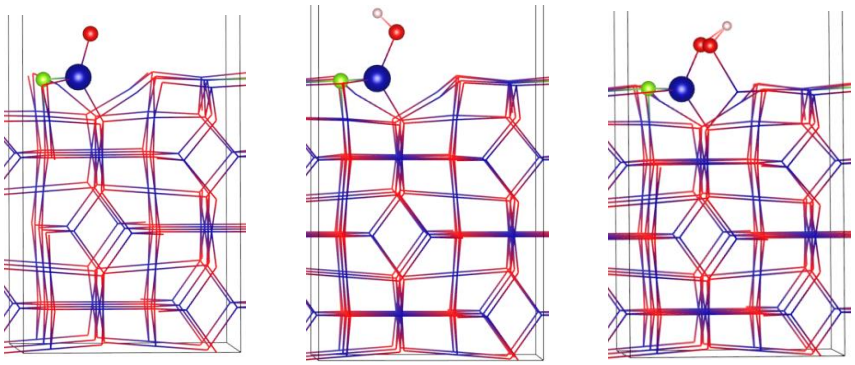

References

1. G. Kresse and J. Furthmiiller, *Comput. Mater. Sci*, 1996, **6**, 15-50.
2. Y. Zhang and W. Yang, *Phys. Rev. Lett.*, 1998, **80**, 890.
3. F. Zasada, J. Gryboś, P. Indyka, W. Piskorz, J. Kaczmarczyk and Z. Sojka, *J. Phys. Chem. C*, 2014, **118**, 19085−19097.
4. M. Methfessel and A. T. Paxton, *Phys. Rev. B*, 1989, **40**, 3616-3621.
5. K. Mathew, V. S. C. Kolluru, S. Mula, S. N. Steinmann and R. G. Hennig, *J. Chem. Phys.*, 2019, **151**, 234101.
6. K. Mathew, R. Sundararaman, K. Letchworth-Weaver, T. A. Arias and R. G. Hennig, *J. Chem. Phys.*, 2014, **140**, 084106.
7. N. Wang, P. Ou, R. K. Miao, Y. Chang, Z. Wang, S. F. Hung, J. Abed, A. Ozden, H. Y. Chen, H. L. Wu, J. E. Huang, D. Zhou, W. Ni, L. Fan, Y. Yan, T. Peng, D. Sinton, Y. Liu, H. Liang and E. H. Sargent, *J. Am. Chem. Soc.*, 2023, **145**, 7829-7836.
8. J. Yu, F. A. Garces-Pineda, J. Gonzalez-Cobos, M. Pena-Diaz, C. Rogero, S. Gimenez, M. C. Spadaro, J. Arbiol, S. Barja and J. R. Galan-Mascaros, *Nat. Commun.*, 2022, **13**, 4341.
9. M. Blasco-Ahicart, J. Soriano-Lopez, J. J. Carbo, J. M. Poblet and J. R. Galan-Mascaros, *Nat. Chem.*, 2018, **10**, 24-30.
10. S. Anantharaj, K. Karthick and S. Kundu, *Inorg. Chem.*, 2019, **58**, 8570-8576.
11. J. Huang, H. Sheng, R. D. Ross, J. Han, X. Wang, B. Song and S. Jin, *Nat. Commun.*, 2021, **12**, 3036.
12. M. Chatti, J. L. Gardiner, M. Fournier, B. Johannessen, T. Williams, T. R. Gengenbach, N. Pai, C. Nguyen, D. R. MacFarlane, R. K. Hocking and A. N. Simonov, *Nat. Catal.*, 2019, **2**, 457-465.
13. L. Chong, G. Gao, J. Wen, H. Li, H. Xu, Z. Green, J. D. Sugar, A. J. Kropf, W. Xu, X.-M. Lin, H. Xu, L.-W. Wang and D.-J. Liu, *Science*, 2023, **380**, 609-616.
14. A. Li, S. Kong, C. Guo, H. Ooka, K. Adachi, D. Hashizume, Q. Jiang, H. Han, J. Xiao and R. Nakamura, *Nat. Catal.*, 2022, **5**, 109-118.
15. S. Kong, A. Li, J. Long, K. Adachi, D. Hashizume, Q. Jiang, K. Fushimi, H. Ooka, J.

Xiao and R. Nakamura, *Nat. Catal.*, 2024, **7**, 252-261.

16. S. Pan, H. Li, D. Liu, R. Huang, X. Pan, D. Ren, J. Li, M. Shakouri, Q. Zhang, M. Wang, C. Wei, L. Mai, B. Zhang, Y. Zhao, Z. Wang, M. Graetzel and X. Zhang, *Nat. Commun.*, 2022, **13**, 2294.

17. I. A. Moreno-Hernandez, C. A. MacFarland, C. G. Read, K. M. Papadantonakis, B. S. Brunschwig and N. S. Lewis, *Energy Environ. Sci.*, 2017, **10**, 2103-2108.

18. S. D. Ghadge, O. I. Velikokhatnyi, M. K. Datta, P. M. Shanthi, S. Tan and P. N. Kumta, *ACS Appl. Energy Mater.*, 2019, **3**, 541-557.

19. F. Hu, S. Zhu, S. Chen, Y. Li, L. Ma, T. Wu, Y. Zhang, C. Wang, C. Liu, X. Yang, L. Song, X. Yang and Y. Xiong, *Adv. Mater.*, 2017, **29**, 1606570.

20. P. P. Patel, M. K. Datta, O. I. Velikokhatnyi, R. Kuruba, K. Damodaran, P. Jampani, B. Gattu, P. M. Shanthi, S. S. Damle and P. N. Kumta, *Sci. Rep.*, 2016, **6**, 28367.

21. J. Wu, M. Liu, K. Chatterjee, K. P. Hackenberg, J. Shen, X. Zou, Y. Yan, J. Gu, Y. Yang, J. Lou and P. M. Ajayan, *Adv. Mater. Interfaces*, 2016, **3**, 1500669.

22. Z. Jiang, W. Zhou, C. Hu, X. Luo, W. Zeng, X. Gong, Y. Yang, T. Yu, W. Lei and C. Yuan, *Adv. Mater.*, 2023, **35**, 2300505.